Combined Bimolecular Fluorescence Complementation and Förster Resonance Energy Transfer Reveals Ternary SNARE Complex Formation in Living Plant Cells[1][W][OA]

Mark Kwaaitaal, Nana F. Keinath[2], Simone Pajonk[3], Christoph Biskup, and Ralph Panstruga*

Max-Planck Institute for Plant Breeding Research, D–50829 Cologne, Germany (M.K., N.F.K., S.P., R.P.); and Universitätsklinikum Jena, D–07740 Jena, Germany (C.B.)

Various fluorophore-based microscopic methods, comprising Förster resonance energy transfer (FRET) and bimolecular fluorescence complementation (BiFC), are suitable to study pairwise interactions of proteins in living cells. The analysis of interactions between more than two protein partners using these methods, however, remains difficult. In this study, we report the successful application of combined BiFC-FRET-fluorescence lifetime imaging microscopy and BiFC-FRET-acceptor photobleaching measurements to visualize the formation of ternary soluble *N*-ethylmaleimide-sensitive factor attachment receptor complexes in leaf epidermal cells. This method expands the repertoire of techniques to study protein-protein interactions in living plant cells by a procedure capable of visualizing simultaneously interactions between three fluorophore-tagged polypeptide partners.

Many biological processes rely on the dynamic assembly and disassembly of multicomponent protein complexes. Experimental methods based on genetically encoded fluorophores are widely used to study the subcellular localization and binary protein-protein interactions in living cells. The subcellular localization of proteins can be visualized by translationally fusing them to fluorophores, which are now available across a wide spectral range (Shaner et al., 2005). Fluorescence microscopy allows imaging and tracing of these proteins in real time in living cells. However, the resolution of a conventional epifluorescence microscope or a confocal laser scanning microscope is insufficient to resolve distances smaller than approximately 200 nm between biological macromolecules and to demonstrate their vicinity at the molecular scale (Bhat et al., 2006; Held et al., 2008).

Two fluorophore-based methods are commonly employed to study protein-protein interactions on the stage of a light microscope and overcome its limitations: bimolecular fluorescence complementation (BiFC; Hu et al., 2002; Bracha-Drori et al., 2004; Walter et al., 2004) and Förster resonance energy transfer (FRET; Hink et al., 2002; Chen et al., 2003; Russinova et al., 2004). The BiFC approach is based on the restoration of an intact fluorophore from its nonfluorescent N- and C-terminal domains. When the two complementing fragments are fused to potentially interacting proteins, close proximity of the proteins can bring the N- and C-terminal fluorophore domains into a favorable position and orientation and thereby facilitate their association into a functional fluorophore (Hu et al., 2002; Kerppola, 2008). Since only standard fluorescence microscopic equipment is required for this technique, it is a popular method to analyze protein-protein interactions (Weinthal and Tzfira, 2009).

An alternative procedure exploits a physical phenomenon referred to as FRET to obtain information about the molecular vicinity of fluorophore-labeled proteins. FRET occurs when a donor fluorophore is brought into close proximity (less than 10 nm) of a suitable acceptor fluorophore. In this case, the donor can transmit its excitation energy to the acceptor. The extent of FRET depends on various parameters, such as the distance between donor and acceptor, their spectral properties, the relative orientation of the donor and acceptor transition dipoles, and the refractive index of the medium (for a more detailed introduction to the theory of FRET, see "Materials and Methods"; Clegg, 1996; Periasamy and Day, 2005; Biskup et al., 2007). The extent of FRET can be estimated by several means, such as by assessing the sensitized emission (Shah et al., 2001, 2002), by determining the donor fluorescence before and after acceptor photobleaching (APB; Bhat et al., 2005), or by measuring the fluores-

[1] This work was supported by the Deutsche Forschungsgemeinschaft (grant no. SFB670).

[2] Present address: Heidelberg Institute for Plant Sciences, Universität Heidelberg, Im Neuenheimer Feld 230, D–69120 Heidelberg, Germany.

[3] Present address: University of Heidelberg, Bioquant BQ23, Im Neuenheimer Feld 267, D–69120 Heidelberg, Germany.

* Corresponding author; e-mail panstrug@mpiz-koeln.mpg.de.

The author responsible for distribution of materials integral to the findings presented in this article in accordance with the policy described in the Instructions for Authors (www.plantphysiol.org) is: Ralph Panstruga (panstrug@mpiz-koeln.mpg.de).

[W] The online version of this article contains Web-only data.

[OA] Open Access articles can be viewed online without a subscription.

www.plantphysiol.org/cgi/doi/10.1104/pp.109.151142

cence lifetime of the donor (Russinova et al., 2004; Bhat et al., 2005; Tonaco et al., 2006; Shen et al., 2007; Osterrieder et al., 2009). Depending on the method, FRET measurements require more or less sophisticated microscopic equipment.

Many biological processes involve protein complexes composed of more than two proteins, which are difficult to study with the experimental approaches outlined above. For example, biologically active *N*-ethylmaleimide-sensitive factor attachment receptor (SNARE) complexes are composed of three distinct protein partners. SNAREs, together with accessory proteins and cytosolic calcium, catalyze membrane fusion events in eukaryotic cells. A binary or ternary t-SNARE complex composed of a Qa-SNARE, also called syntaxin, and Qb- and Qc-SNARE domains present in either one protein (synaptosome-associated protein [SNAP-25]) or as two separate units is located at the target membrane. This t-SNARE complex interacts with an R-SNARE (vesicle-associated membrane protein [VAMP]) present on the vesicle, and the formation of the fusogenic SNARE complex brings the opposing membranes into close proximity (Jahn and Scheller, 2006; Leabu, 2006). Besides their role in cellular homoeostasis, SNAREs play a major role in various plant biological processes, such as cytokinesis, gravitropism, and defense against pathogens (Lipka et al., 2007).

The orthologous Arabidopsis (*Arabidopsis thaliana*) and barley (*Hordeum vulgare*) syntaxins, AtPEN1 and HvROR2, respectively, are essential in restricting the invasion of nonadapted powdery mildew species or in broad-spectrum powdery mildew resistance conferred by loss-of-function *mlo* mutants, respectively (Collins et al., 2003; Assaad et al., 2004). Both syntaxins form a binary t-SNARE complex with the orthologous SNAP-25-like proteins AtSNAP33 and HvSNAP34 (Collins et al., 2003; Kwon et al., 2008), which in turn interact with the R-SNAREs AtVAMP721/AtVAMP722 and HvVAMP721, respectively, by adopting an authentic ternary SNARE complex (Kwon et al., 2008). In addition to a range of other polypeptides, the mentioned Arabidopsis and barley SNARE partners focally accumulate below the site of attempted fungal penetration (Assaad et al., 2004; Bhat et al., 2005; Kwon et al., 2008), which probably precedes their extracellular deposition in the paramural space (Meyer et al., 2009).

In this study, we combined BiFC-FRET measurements based on cerulean fluorescent protein (CrFP; Rizzo et al., 2004) as a donor and reconstituted yellow fluorescent protein (YFP; Walter et al., 2004; Schütze et al., 2009) as an acceptor to study the formation of a ternary protein assembly. We concentrated on the well-characterized SNARE complexes described above that play a decisive role in antifungal defense. FRET was detected by measuring the fluorescence lifetime of the donor in each pixel of the sample in a fluorescence lifetime imaging (FLIM) setup. Occurrence of FRET was corroborated by APB experiments. Our data demonstrate the technical feasibility of combined BiFC-FRET-FLIM and BiFC-FRET-APB assays to study ternary protein complexes in living plant cells.

RESULTS

HvROR2 Is Present in Large SDS-Resistant, Heat-Sensitive Protein Complexes

Binary interactions between HvROR2, HvSNAP34, and HvVAMP721 have been demonstrated previously (Collins et al., 2003; Kwon et al., 2008). Before assessing ternary SNARE complex formation by BiFC and FRET, we aimed to demonstrate HvROR2-containing ternary complexes in barley. In analogy to experiments performed by Kwon et al. (2008), we detected the presence of HvROR2-containing SDS-resistant, heat-sensitive ternary SNARE complexes by biochemical means in 7-d-old barley leaves (Fig. 1). Thus, like its ortholog AtPEN1, HvROR2 forms ternary SNARE complexes in vivo.

Colocalization of Fluorophore-Tagged SNARE Fusion Proteins in Epidermal Cells

We studied the subcellular localization of the barley SNAREs HvSNAP34, HvROR2, and HvVAMP721 by expression of fluorophore-tagged versions of these proteins in barley leaf epidermal cells. Owing to the longevity of detached barley leaves used for transformation, lower autofluorescence levels, and higher expression levels, we performed most experiments of this study in this species and validated essential observations in Arabidopsis. The translational fusion variants of CrFP (Rizzo et al., 2004) to the N termini of HvROR2 (CrFP-HvROR2) or HvVAMP721 (CrFP-HvVAMP721) predominantly localized to the cell pe-

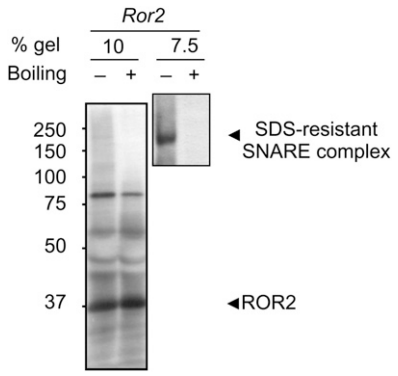

Figure 1. The HvROR2 protein is present in heat-sensitive, but SDS-resistant, complexes in barley leaves. Total protein extracts were prepared from barley wild-type leaves. Following SDS-PAGE (50 μg lane^{-1}) on either 10% or 7.5% gels, HvROR2 was detected by immunoblot using an anti-HvROR2 antiserum (Collins et al., 2003). The 10% gel allows visualization of the HvROR2 monomer, while the 7.5% gel illustrates the high-M_r HvROR2-containing complexes. Note the absence of these complexes upon boiling of the sample prior to gel loading.

riphery, most likely the plasma membrane (PM; Fig. 2, A and B). Aside from the PM, CrFP-HvROR2 and in particular CrFP-HvVAMP721 were often visible in mobile spots close to the PM (Supplemental Fig. S1, A and B). The C-terminal fusion of HvSNAP34 with CrFP (HvSNAP34-CrFP) was predominantly present at the cell periphery but also visible in cytoplasmic areas (Fig. 2C). We observed similar subcellular localizations for the Arabidopsis SNAREs AtPEN1, AtSNAP33, and AtVAMP722 upon coexpression of fluorophore-tagged versions of these proteins in epidermal cells of Arabidopsis rosette leaves (compare Fig. 2, A–C, with Supplemental Fig. S4, A–C, and Supplemental Fig. S1, A and B, with Supplemental Fig. S1, C and D).

Analysis of Pairwise Interaction of SNARE Proteins Using the BiFC Assay

Pairwise interactions between either the above-mentioned barley SNAREs or their Arabidopsis orthologs were previously revealed in yeast two-hybrid studies and in planta by FRET-FLIM analysis and biochemical methods (Collins et al., 2003; Kwon et al., 2008; Pajonk et al., 2008). With the ultimate goal to visualize ternary protein-protein interactions, we first aimed at corroborating these binary interactions using the BiFC assay (Hu et al., 2002; Bracha-Drori et al., 2004; Walter et al., 2004). Fusions of interacting proteins with split YFP halves that are able to form a functional fluorophore can then serve as an acceptor in FRET experiments involving a third interaction partner, which is fused to CrFP as donor fluorophore. Translational fusions of the SNARE partners to nonfluorescent N- and C-terminal halves of YFP were coexpressed in barley leaf epidermal cells, and restoration of YFP fluorescence was assessed. We tested all possible pairwise combinations of translational fusions of the split YFP halves to the SNARE proteins by epifluorescence microscopy-based detection of the YFP signal (Supplemental Fig. S2). We noted that only a few tested combinations (e.g. a fusion of the N-terminal half of YFP [^{N}YFP] to the N terminus of HvROR2 [^{N}YFP-HvROR2] coexpressed with a fusion of the C-terminal half of YFP [^{C}YFP] to the C terminus of HvSNAP34 [HvSNAP34-^{C}YFP]) provided bright BiFC fluorescence, suggesting that in these fusion protein pair constellations the fluorophore halves are in a sterical orientation that is favorable for complementation of the YFP fluorophore. In the subsequent analysis, we focused on these fusion protein combinations, because only intact functional YFP fluorophores can act as an acceptor in FRET experiments.

Examination by confocal laser scanning microscopy of the BiFC couples with the brightest YFP fluorescence (Fig. 2, D–F) revealed that the interacting proteins were not as evenly distributed at the PM as in the case of the single proteins but were often present in large clusters of vesicle-like compartments (VLCs; arrows in Fig. 2, D–F). Coexpression of ^{N}YFP-HvROR2 together with HvSNAP34-^{C}YFP and ^{N}YFP-HvVAMP721 with HvSNAP34-^{C}YFP resulted in VLCs that were larger and showed more intense fluorescence than in case of ^{N}YFP-HvROR2 coexpressed with ^{C}YFP-HvVAMP721 (Fig. 2, compare D with E and F). Although weaker than in the VLCs, YFP fluorescence could still be observed at the cell periphery (Supplemental Fig. S1, E and

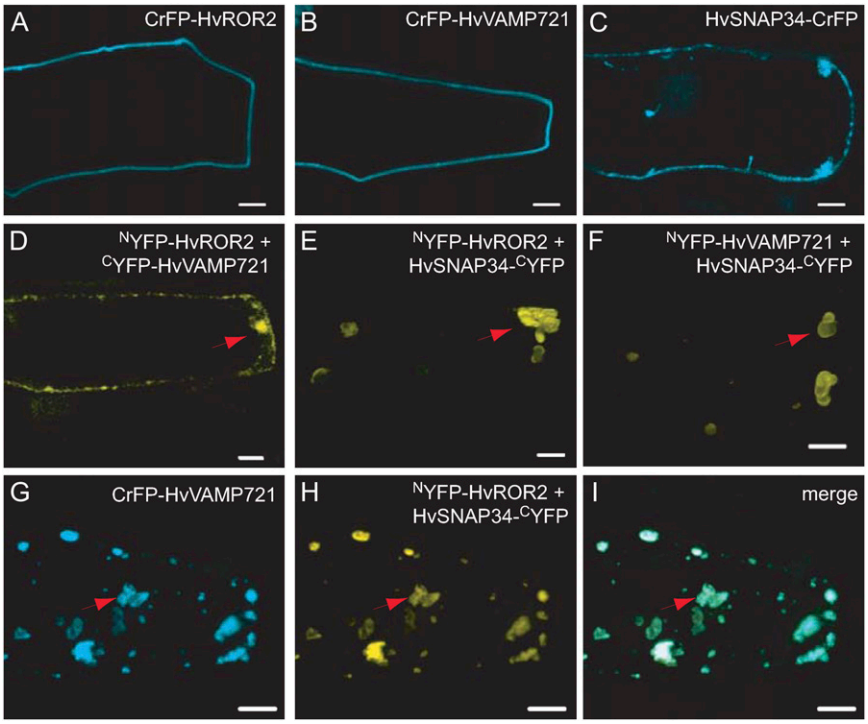

Figure 2. Coexpression of HvROR2, HvSNAP34, and HvVAMP721 in barley epidermal cells results in clustering of VLCs containing the three complementary SNARE partners. A to C, CrFP fluorescence micrographs of cells expressing CrFP-HvROR2 (A), CrFP-HvVAMP721 (B), or HvSNAP34-CrFP (C). D, YFP fluorescence micrograph of a cell expressing the BiFC couple ^{N}YFP-HvROR2 and ^{C}YFP-HvVAMP721. E and F, Micrographs (projection of a z-stack) of cells coexpressing ^{N}YFP-HvROR2 and HvSNAP34-^{C}YFP (E) or ^{N}YFP-HvVAMP721 and HvSNAP34-^{C}YFP (F). G to I, Micrographs (projection of a z-stack) of a cell coexpressing CrFP-HvVAMP721 with the BiFC couple ^{N}YFP-HvROR2 and HvSNAP34-^{C}YFP. G, CrFP fluorescence. H, YFP fluorescence of complemented YFP. I, Merged image of all channels. The arrows mark clustered vesicle-like structures. Bars = 10 μm.

F). Analysis of the pairwise interactions of the Arabidopsis SNAREs in Arabidopsis epidermal cells using the BiFC system revealed a comparable interaction pattern as for the barley SNAREs (Supplemental Fig. S4, D–F).

Coexpression of Three Complementary SNARE Partners

Next, we coexpressed all three SNARE partners in barley leaf epidermal cells. In this experiment, one SNARE protein was expressed as a translational fusion to CrFP and the other two as a split YFP couple (translationally fused to ^{N}YFP and ^{C}YFP, respectively). In all tested combinations, the three SNARE partners completely colocalized in large clusters of VLCs (Fig. 2, G–I), suggesting that intermolecular interactions promote and/or stabilize higher order SNARE protein assemblies. The size of the VLC clusters harboring all three SNARE partners was variable and ranged from less than 1 μm to approximately 10 μm. We noted no preferential site at which VLC clusters formed inside the barley epidermal cells. To investigate the nature of the SNARE protein-induced VLCs further, we coexpressed a set of barley proteins known to reside in the PM as mCherry-tagged (Shu et al., 2006) fusion proteins with CrFP-HvVAMP721, ^{N}YFP-HvROR2, and HvSNAP34-^{C}YFP in barley epidermal cells. This revealed that all tested barley integral membrane proteins coaccumulated, to varying degrees, with the SNAREs at or in the VLC clusters, suggesting that the majority of PM-targeted proteins may completely or partially accumulate at or in the SNARE-induced VLCs (Supplemental Fig. S3).

The fact that only a few tested combinations (e.g. ^{N}YFP-HvROR2 coexpressed with ^{C}YFP-HvVAMP721) provided a significant BiFC signal already shows that BiFC formation is very specific and requires the two halves to be in close proximity and a favorable orientation. To further exclude that unspecific BiFC signals can be induced by high local concentration of the fluorescent halves, we coexpressed barley cytochrome *b*561 (a non-SNARE protein coaccumulating in VLCs; Supplemental Fig. S3, M–P) as a BiFC partner (HvCytb561-^{C}YFP) with ^{N}YFP-HvROR2 and CrFP-HvVAMP721. This combination also induced the formation of VLCs, but without any detectable YFP signal (Supplemental Fig. S3, Q–S), which suggests that the N- and C-terminal halves of the split YFP molecule do not even complement at high local concentrations of labeled PM-resident proteins in the VLCs and do not elicit unspecific BiFC signals.

As in case of their barley counterparts, coexpression of CrFP-AtVAMP722, ^{N}YFP-AtPEN1, and AtSNAP33-^{C}YFP resulted in coaccumulation of the three SNARE partners in randomly distributed VLC clusters of variable size (Supplemental Fig. S4, G–I). This indicates that the formation of SNARE-induced polypeptide clusters is not a species-specific phenomenon but that the formation of VLC clusters can occur in cells of monocotyledonous as well as dicotyledonous plants. A membrane-targeted form of CrFP, generated by fusing a CAAX box (CTIL; Thompson and Okuyama, 2000) to the fluorophore, localized next to other cellular compartments and the PM to the VLCs, which suggests that abundant membrane material is present in the VLCs (Supplemental Fig. S4, N–Q). This supports the notion that these compartments are derived from membrane/vesicle fusion events. Notably, even despite high expression levels of the complementary SNARE partner proteins and their clustering in VLCs, the SNARE proteins retained an authentic posttrans-

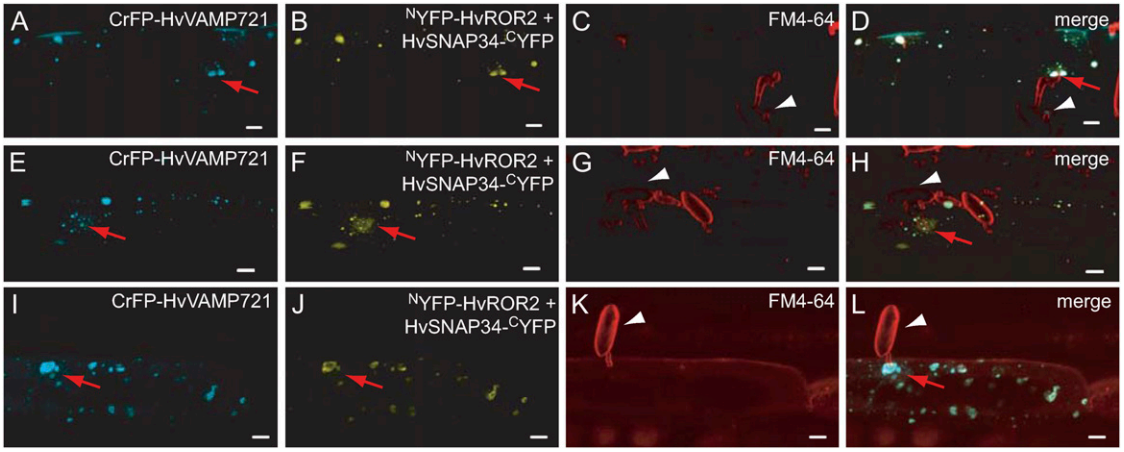

Figure 3. Coexpressed SNAREs HvROR2, HvSNAP34, and HvVAMP721 retain their dynamics following powdery mildew challenge. Micrographs (projection of a z-stack) of a FM 4-64-stained cell coexpressing CrFP-HvVAMP721 with the BiFC couple ^{N}YFP-HvROR2 and HvSNAP34-^{C}YFP at 16 to 20 h after challenge with *Bgh*. A, E, and I, CrFP fluorescence. B, F, and J, Fluorescence of complemented YFP. C, G, and K, FM 4-64 fluorescence. D, H, and L, Merged images of all channels. The red arrows point at the focal accumulation of SNARE proteins below the appressorial germ tube, and the white arrowheads point at the fungal spore from which the respective germ tube emerges. Bars = 10 μm.

lational dynamic response to powdery mildew attack by focally coaccumulating below the site of attempted fungal penetration (Fig. 3).

A documented weakness of the BiFC assay is that the complemented YFP, once formed, does not disassemble, which stabilizes the entire protein complex (Hu et al., 2002; Held et al., 2008; Kerppola 2008). To exclude the possibility that protein complex stabilization by the BiFC system caused the observed clustering phenomenon, we coexpressed the three SNARE partners tagged with distinct full-size monomeric fluorophores (CrFP-AtVAMP722, mYFP-AtPEN1, and AtSNAP33-mCherry; for mYFP, Zacharias et al., 2002; for mCherry, Shu et al., 2006) in Arabidopsis epidermal cells. Coexpression of these fusion proteins resulted in an accumulation pattern of all three SNAREs in clusters of VLCs that were indistinguishable from the BiFC-associated VLCs (Supplemental Fig. S4, J–M). This demonstrates that the formation of the VLCs and the colocalization of the SNARE proteins are not caused by the use of the BiFC system.

Visualization of in Vivo Ternary SNARE Complex Formation by Combined BiFC-FRET-FLIM Analysis

To further characterize the reconstituted YFP fluorophore, we measured and compared the fluorescence emission spectra and fluorescence lifetime of YFP, YFP N-terminally fused to HvROR2 (YFP-HvROR2), and the reconstituted YFP of the ^{N}YFP-HvROR2 and HvSNAP34-^{C}YFP BiFC couple expressed in barley leaf epidermal cells. Consistent with previous publications (Hu et al., 2002), the fluorescence emission spectra of translationally fused and reconstituted YFP were indistinguishable from native YFP (Supplemental Fig. S5A). In the FLIM experiment, the fluorescence decay curves were fitted with a monoexponential decay model (Kremers et al., 2006). We found an average fluorescence lifetime for YFP of $\overline{\tau_m^c}$ = 3.06 ± 0.06 ns (mean ± SD), which is similar to published values (Kremers et al., 2006). For YFP-HvROR2, $\overline{\tau_m^c}$ was 2.92 ± 0.09 ns, and for reconstituted YFP, $\overline{\tau_m^c}$ was 2.74 ± 0.08 ns (Table I; Supplemental Fig. S5B). Given that the barrel structure of native YFP and the associated YFP halves might be divergent, these values are surprisingly similar and in the range of the lifetime difference between CrFP and enhanced cyan fluorescent protein, which differ by only three amino acids (Rizzo et al., 2004). Taken together, these data suggest that the reconstituted YFP fluorophore is likely to function as a suitable acceptor molecule.

To assess if all three SNARE partners were in molecular proximity to each other and formed a genuine ternary SNARE complex, we tested if FRET occurred between CrFP donor molecules and different complemented YFP acceptor molecules (for variations in complex formation where FRET, BiFC, or BiFC-FRET can or cannot occur, see scheme in Fig. 4A). The extent of FRET was determined by FLIM (for details, see "Materials and Methods"). For each series of experiments, we determined the average fluorescence lifetime $\overline{\tau_m^c}$ of the donor in the absence of an acceptor (negative control) and compared the result with $\overline{\tau_m^c}$ of the donor coexpressed with various BiFC acceptor combinations.

A monoexponential decay model was sufficient to fit the CrFP fluorescence decay and therefore was used for the analysis of the donor-alone measurements (Supplemental Materials and Methods S1). $\overline{\tau_m^c}$ for CrFP-HvVAMP721 in barley leaf epidermal cells was 2.49 ± 0.09 ns (mean ± SD; Fig. 4, B, C, and J; Table I). However, to adequately fit the fluorescence decay observed upon coexpression of CrFP-HvVAMP721 with ^{N}YFP-HvROR2 and HvSNAP34-^{C}YFP, a biexponential model was used (Fig. 4, D–F and J; Table I). The fit yielded $\overline{\tau_m^c}$ = 2.16 ± 0.19 ns, which is significantly

Table I. *Fluorescence lifetimes and energy transfer efficiencies*

The fluorescence lifetime of the donor CrFP or YFP was determined in barley or Arabidopsis epidermal cells transiently expressing the mentioned constructs and compared with the donor-alone lifetime. From the average fluorescence lifetimes $\overline{\tau_m^c}$, the FRET efficiency E value was calculated according to Equation 2 (see "Materials and Methods").

Donor	Acceptor	$\overline{\tau_m^c}$ ± SD[a]	E ± SD[b]	No.[c]	P[d]
CrFP-HvVAMP721	–	2.49 ± 0.09	–	26	–
CrFP-HvVAMP721	^{N}YFP-HvROR2 + HvSNAP34-^{C}YFP	2.16 ± 0.19	12.9 ± 5.7	23	<0.001
CrFP-HvVAMP721	^{N}YFP-HvROR2 + ^{C}YFP-HvSNAP34	2.44 ± 0.13	2.6 ± 4.7	15	0.58
HvSNAP34-CrFP	–	2.54 ± 0.11	–	10	–
HvSNAP34-CrFP	^{N}YFP-HvROR2 + ^{C}YFP-HvVAMP721	2.47 ± 0.08	3.2 ± 1.9	11	0.08
CrFP-HvROR2	–	2.50 ± 0.09	–	13	–
CrFP-HvROR2	^{N}YFP-HvVAMP721 + HvSNAP34-^{C}YFP	2.42 ± 0.05	4.5 ± 3.1	19	0.01
CrFP-AtVAMP722	–	2.55 ± 0.10	–	21	–
CrFP-AtVAMP722	^{N}YFP-AtPEN1 + AtSNAP33-^{C}YFP	2.24 ± 0.18	11.4 ± 6.2	27	<0.001
–	YFP	3.06 ± 0.06	–	13	–
–	YFP-HvROR2	2.92 ± 0.09	–	11	<0.001[e]
–	^{N}YFP-HvROR2 + HvSNAP34-^{C}YFP	2.74 ± 0.08	–	13	<0.001[e]; <0.001[f]

[a]Average mean lifetime $\overline{\tau_m^c}$ (ns) ± SD. [b]Fluorescence energy transfer (%) ± SD, calculated according to Equation 2 (see "Materials and Methods"). [c]Number of cells analyzed. [d]P value according to Student's t test (compared with donor-alone lifetime). [e]P value according to Student's t test (compared with YFP lifetime). [f]P value according to Student's t test (compared with YFP-HvROR2 lifetime).

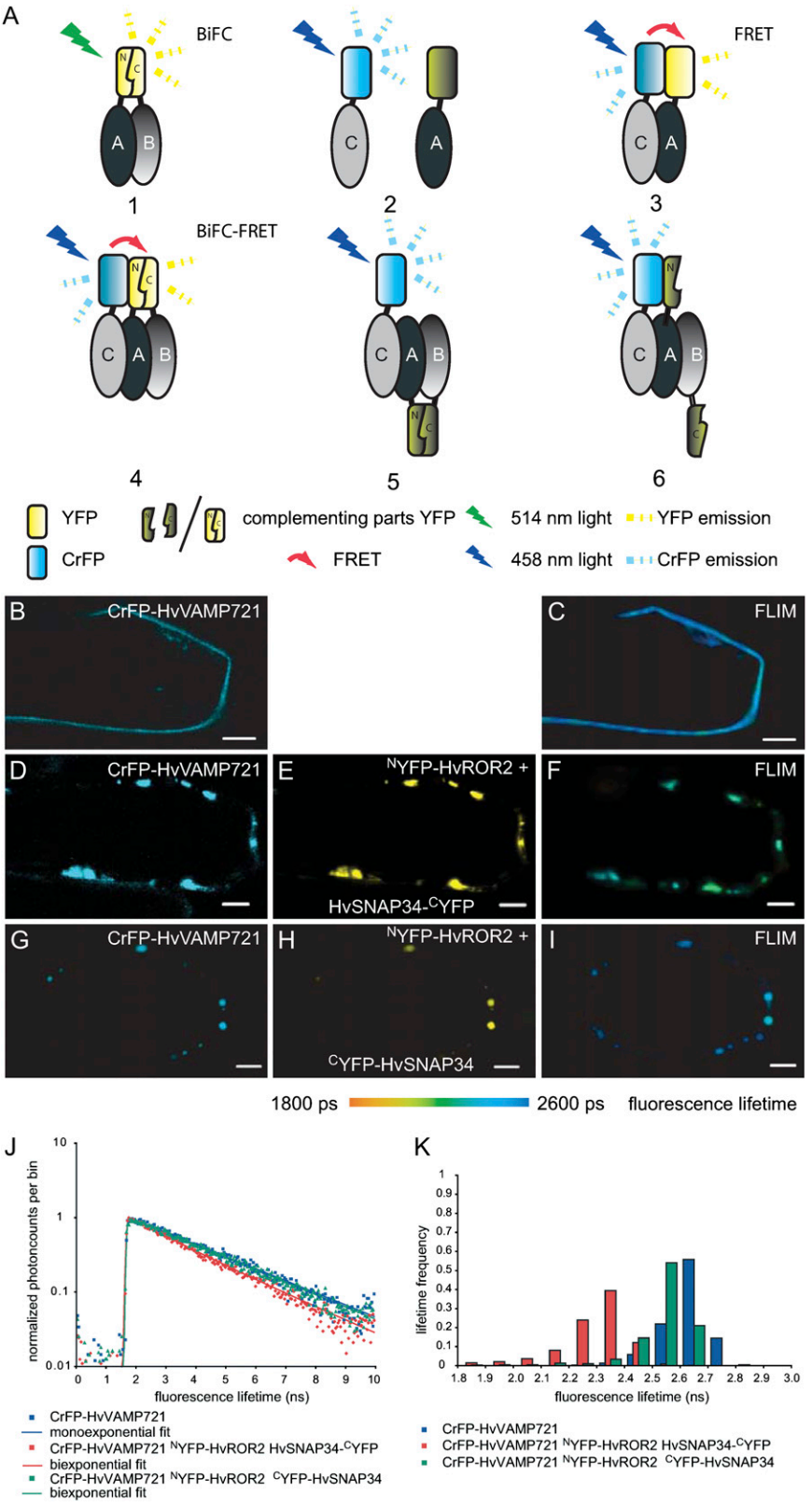

Figure 4. In planta visualization of ternary SNARE complex formation by combined BiFC-FRET-FLIM in barley leaf epidermal cells. A, Schematic representations of BiFC, FRET, and BiFC-FRET revealing possible scenarios where FRET can (scenarios 3 and 4) or cannot (scenarios 1, 2, 5, and 6) occur between a donor and an acceptor molecule, which depends on the presence of a suitable acceptor and a favorable distance (5–10 nm) between donor and acceptor molecules. Scenario 4 illustrates the principle of BiFC-FRET. YFP reconstitutes when proteins A and B fused to the N- and C-terminal parts of YFP, respectively, are in close proximity to each other and expose their split YFP domains suitably. The CrFP donor attached to protein C is excited by 458-nm laser light and can transfer its excitation energy to the reconstituted YFP if the protein-protein interaction positions them close together (less than 10 nm). B and C, Fluorescence micrographs of a cell expressing CrFP-HvVAMP721. B, CrFP fluorescence. C, Color-coded CrFP fluorescence lifetime image. Fluorescence lifetimes determined in each pixel are encoded by color according to the color scale shown at the bottom. D to F, Fluorescence micrographs of a cell coexpressing CrFP-HvVAMP721 with the BiFC couple ^{N}YFP-HvROR2 and HvSNAP34-^{C}YFP. D, CrFP fluorescence. E, Fluorescence of complemented YFP. F, Color-coded CrFP fluorescence lifetime image. G to I, Fluorescence micrographs of a cell coexpressing CrFP-HvVAMP721 with the BiFC couple ^{N}YFP-HvROR2 and ^{C}YFP-HvSNAP34. G, CrFP fluorescence. H, Fluorescence of complemented YFP. I, Color-coded CrFP fluorescence lifetime image. Bars = 10 μm. J and K, Representative normalized fluorescence decay curves (J) and CrFP lifetime histograms (K) obtained from FLIM measurements in barley epidermal cells expressing CrFP-HvVAMP721 alone (blue) CrFP-HvVAMP721 with ^{N}YFP-HvROR2 and HvSNAP34-^{C}YFP (red), and CrFP-HvVAMP721 with ^{N}YFP-HvROR2 and ^{C}YFP-HvSNAP34 (green). Donor-alone fluorescence decay curves were fitted using a monoexponential model, whereas the fluorescence decay in the presence of an acceptor fluorophore had to be fitted with a biexponential model. The second lifetime component was fixed to the average donor lifetime measured in control experiments. The lifetime histograms were generated using a bin size of 100 ps.

lower than the control values, indicating effective energy transfer between the CrFP donor molecule and the reconstituted split YFP acceptor molecule. Analysis of the lifetime decay curves with a monoexponential decay model for both the donor-alone and donor-plus-acceptor studies also revealed a significant

$\overline{\tau_m^c}$ reduction for CrFP-HvVAMP721 with ^{N}YFP-HvROR2 and HvSNAP34-^{C}YFP (2.19 ± 0.17 ns) compared with CrFP-HvVAMP722 alone as well (Supplemental Table S1). This control excludes that the observed lifetime reduction is caused by the chosen decay model. The variation in fluorescence lifetime (τ_m) throughout an individual cell (Fig. 4F) and the variation in lifetimes $\overline{\tau_m^c}$ averaged over all measured cells (Table I) likely reflect the dynamic nature of the interaction between the three SNARE partners. From the lifetime data, an average FRET efficiency of 12.9% ± 5.7% (mean ± SD; Eq. 2 in "Materials and Methods") was calculated.

To assess if the reduction of the donor lifetime was only caused by FRET and not by any other photophysical phenomena, such as quenching or photoconversion, APB experiments were performed in a small area of the cell followed by a second FLIM measurement in the same region (Fig. 5, A–G). After APB, YFP fluorescence was almost undetectable (compare the marked areas in Fig. 5A with Fig. 5B; see also Fig. 5E), and a concomitant increase in CrFP fluorescence was observed in the bleached area (compare marked areas in Fig. 5C with Fig. 5D; see also Fig. 5E). From the increase in CrFP intensity in this example, a FRET efficiency of 11.2% (Eq. 1 in "Materials and Methods") was calculated, which is similar to the FRET efficiency determined from the lifetime values (see above and Table I). APB measurements on multiple cells yielded an average FRET efficiency of 13.2% ± 7.1% (n = 10) and showed, similar to the lifetime values, considerable variation between individual cells and experiments. Thus, consistent with other studies (Orthaus et al., 2008), APB yielded similar results as FLIM. Hence, the more widely available APB method can be used as an alternative to FLIM to determine FRET between CrFP and a reconstituted YFP.

Following APB, also the CrFP lifetime in the bleached area (τ_m^b) increased (compare marked areas in Fig. 5, F and G; Supplemental Fig. S5E). Average lifetimes τ_m^b increased from 2.22 ± 0.11 ns to 2.43 ± 0.04 ns after APB in the bleached area. The average postbleach lifetime differed significantly from prebleach values ($\overline{\tau_m^c}$ of 2.51 ± 0.09 ns [$P < 0.001$]; Table II) and represents a nearly complete recovery to donor-alone values. In conclusion, this experiment confirms that the observed decrease of donor fluorescence lifetime can be attributed to FRET and not to any other photophysical effect that might equally cause a decrease of the donor lifetime.

Positioning of the split ^{C}YFP tag to the N terminus instead the C terminus of HvSNAP34 (^{C}YFP-HvSNAP34) and coexpression with CrFP-HvVAMP721 and ^{N}YFP-HvROR2 resulted in lifetimes similar to the donor molecule alone ($\overline{\tau_m^c}$ = 2.44 ± 0.13 ns; Fig. 4, G–I; Table I), indicating the absence of FRET. However, cells expressing ^{C}YFP-HvSNAP34 and ^{N}YFP-HvROR2 showed clearly visible YFP fluorescence, which excludes the possibility that the absence of a suitable

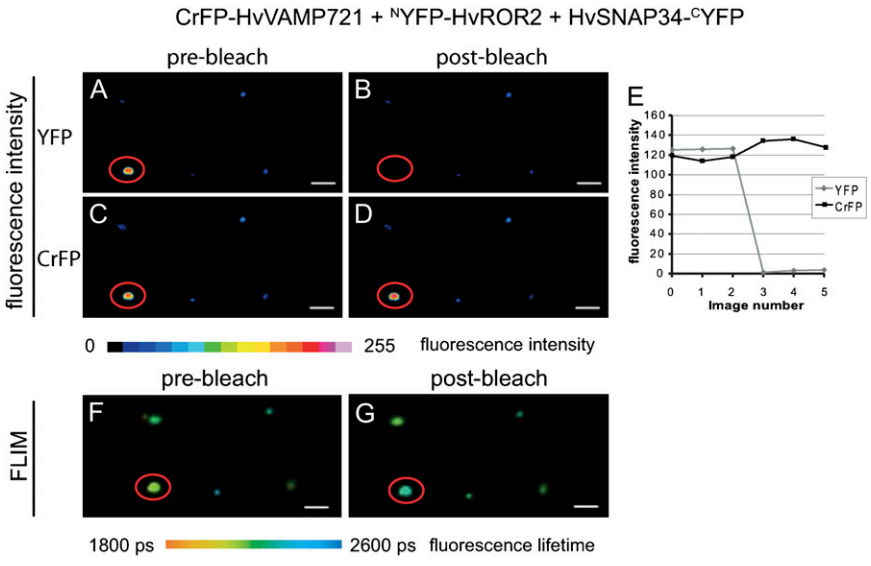

Figure 5. APB confirms FRET between CrFP and the reconstituted YFP. APB experiments were performed to visualize FRET between CrFP-HvVAMP721 and the BiFC couple ^{N}YFP-HvROR2 and HvSNAP34-YFP^C. A to D, False color-coded micrographs of YFP fluorescence intensity before bleaching (A), YFP fluorescence after bleaching (B), CrFP fluorescence before bleaching (C), and CrFP fluorescence after bleaching (D). Fluorescence intensities are color coded according to the scale below the panels. E, Time course of fluorescence intensities during the experiment. Note that CrFP fluorescence increases concomitant to the decrease of YFP fluorescence, indicating that FRET occurred between the fluorophores. F and G, Fluorescence lifetime images of the same cell before (F) and after (G) bleaching. Red circles mark the bleached area. Fluorescence lifetimes determined in each pixel are encoded by color according to the color scale shown at the bottom. Bars = 10 μm.

Table II. *Fluorescence lifetime and energy transfer efficiency determined after photobleaching of the acceptor fluorophore*

To verify that the observed decrease of fluorescence lifetime was only due to FRET, the complemented YFP was bleached in a selected area and the fluorescence lifetimes before and after bleaching were determined. At the same time, the APB experiments served as an independent method to determine the FRET efficiency between the CrFP donor and complemented YFP acceptor molecules.

Donor	Acceptor	$\overline{\tau_m^c}$ ± SD[a]	E ± SD[b]	No.[c]	P[d]
CrFP-HvVAMP721	–	2.51 ± 0.09	–	12	–
CrFP-HvVAMP721[e]	^{N}YFP-HvROR2 + HvSNAP34-^{C}YFP	2.22 ± 0.11	11.5 ± 4.4	11	<0.001
CrFP-HvVAMP721[f]	^{N}YFP-HvROR2 + HvSNAP34-^{C}YFP	2.43 ± 0.04	3.3 ± 1.7	11	<0.001[g]
CrFP-HvVAMP721[h]	^{N}YFP-HvROR2 + HvSNAP34-^{C}YFP	–	13.2 ± 7.1	10	–

[a]Average mean lifetime $\overline{\tau_m^c}$ (ns) ± SD. [b]Fluorescence energy transfer (%) ± SD, calculated according to Equation 2 (see "Materials and Methods"). [c]Number of cells analyzed. [d]P value according to Student's t test (compared with donor-alone lifetime). [e]Lifetime and energy transfer values in the bleached area before photobleaching. [f]Lifetime and energy transfer values in the bleached area after photobleaching. [g]P value according to Student's t test (compared with prebleach lifetime). [h]Energy transfer efficiency determined using the CrFP fluorescence intensity before and after bleaching and Equation 1 (see "Materials and Methods").

acceptor molecule is the reason for the lack of FRET. The presence of FRET in the former and the absence of efficient FRET in the latter combination of the three SNARE partners are further illustrated by representative decay curves and donor lifetime histograms (Fig. 4, J and K).

To assess SNARE complex formation further, we swapped donor and acceptor molecules in the FRET measurements. When CrFP-HvROR2 was combined with the fluorescent BiFC couple ^{N}YFP-HvVAMP721 and HvSNAP34-^{C}YFP, only a small reduction in $\overline{\tau_m^c}$ (2.42 ± 0.05 ns) was observed compared with the donor alone (2.50 ± 0.09 ns; Table I; Supplemental Fig. S6, A–E). Likewise, the HvSNAP34-CrFP donor in combination with ^{N}YFP-HvROR2 and ^{C}YFP-HvVAMP721 yielded only a minor reduction in $\overline{\tau_m^c}$ (2.47 ± 0.08 ns) compared with the donor alone (2.54 ± 0.11 ns; Table I; Supplemental Fig. S6, F–J). The absence of a lifetime reduction upon changing the position of the separate YFP parts or an exchange of the CrFP-labeled donor molecules was likely the consequence of unfavorable distances or orientations between the fluorescent labels (Fig. 4A, scenario 5). However, this finding supports the notion that the $\overline{\tau_m^c}$ reduction observed in cells expressing CrFP-HvVAMP721, ^{N}YFP-HvROR2, and HvSNAP34-YFP^{C} is due to molecular interactions and not molecular crowding, CrFP bleaching, or other phenomena.

Visualization of the Arabidopsis AtPEN1, AtSNAP33, and AtVAMP722 Ternary SNARE Complex in Vivo by BiFC-FRET-FLIM

To examine the applicability of the BiFC-FRET-FLIM approach in another plant species, we also studied complex formation between CrFP-AtVAMP722, ^{N}YFP-AtPEN1, and AtSNAP33-^{C}YFP in Arabidopsis. The three proteins were coexpressed in Arabidopsis epidermal cells, and FLIM measurements were performed. The donor CrFP-AtVAMP722 alone had an average fluorescence lifetime $\overline{\tau_m^c}$ of 2.55 ± 0.10 ns (Table I; Supplemental Fig. S7B). When CrFP-HvVAMP721 was coexpressed with the acceptor couple ^{N}YFP-AtPEN1 and AtSNAP33-^{C}YFP, which as in the case of the respective barley orthologs led to reconstitution of YFP, $\overline{\tau_m^c}$ decreased to 2.24 ± 0.18 ns (Table I; Supplemental Fig. S7, C–E). These results show that BiFC-FRET-FLIM can also be applied to study ternary SNARE complex formation in Arabidopsis leaf epidermal cells and suggest that the method is applicable to a broad range of plant species.

DISCUSSION

BiFC Combined with FRET Reveals the Formation of Ternary SNARE Complexes in Living Plant Cells

In this work, we applied BiFC and BiFC combined with FRET to study the pairwise and ternary interactions, respectively, between a set of complementary barley and their orthologous Arabidopsis SNARE proteins that were previously shown to be essential in disease resistance and plant development (Heese et al., 2001; Collins et al., 2003; Assaad et al., 2004; Zhang et al., 2007; Kwon et al., 2008; Pajonk et al., 2008). Our results corroborate the biochemical detection of these SNARE complexes (Fig. 1; Kwon et al., 2008; Pajonk et al., 2008) and indicate that the biochemically isolated SNARE complexes were not artificially formed during the protein extraction procedure.

To investigate the formation of ternary SNARE complexes, FLIM measurements were performed in epidermal leaf cells coexpressing two SNAREs as BiFC partners (reconstituting a functional YFP acceptor molecule) and the third SNARE fused to CrFP as FRET donor. In the cases where CrFP-HvVAMP721 was used as donor molecule with a YFP reconstituted from ^{N}YFP-HvROR2 and HvSNAP34-^{C}YFP as acceptor, a significant decrease of the fluorescence lifetime ($\overline{\tau_m^c}$), indicative of effective FRET, was observed (Fig. 4F; Table I). Similar results were obtained in the Arabidopsis system (Table I; Supplemental Fig. S7E). However, a significant decrease of $\overline{\tau_m^c}$ only occurred when a C-terminal fusion of HvSNAP34 to ^{C}YFP was

used, while we observed no FRET when an N-terminal fusion of HvSNAP34 to ^{C}YFP was tested (Fig. 4I; Table I). This result may indicate that the two SNARE domains of HvSNAP34 preferentially adopt an antiparallel orientation (Weninger et al., 2003). Additionally, when either CrFP-HvROR2 or HvSNAP34-CrFP was used as a donor molecule, no reduction in $\overline{\tau_m^c}$ occurred (Table I; Supplemental Fig. S6, E and J). When conventional (full-size) fluorophores are employed, FRET can be typically observed in reciprocal experiments with the donor and acceptor fluorophores swapped between the interacting partners (Russinova et al., 2004). However, next to the distance, FRET depends on the dipole orientation of the fluorophores. The use of the BiFC system limits the rotational freedom of the YFP molecule, because the two YFP halves are attached to two interacting partners. This decreases the chance that the CrFP and YFP molecules are properly aligned for FRET to occur (Dale et al., 1979; Chen et al., 2003). By switching the position of the YFP halves fused to the SNAREs, the position of the "fixed" YFP moiety changes, which may provide a plausible explanation for the fact that we did not detect FRET in certain donor/acceptor combinations (Fig. 4A, scenarios 4 and 5). These requirements for fluorophore positioning and orientation as well as the limited rotational freedom of reconstituted YFP suggest that FRET efficiencies determined in a BiFC-FRET three-component system will possibly be lower than for a binary FRET assay.

The finding that the FRET efficiency determined for the ternary SNARE complex is comparable to the efficiency for respective binary SNARE complexes (Table I; Kwon et al., 2008) indicates that the capacity of complemented YFP to serve as a FRET acceptor can equal that of native YFP under favorable conditions. APB confirmed the results of the fluorescence lifetime-based FRET assays. By performing a second FLIM measurement after bleaching, we showed that the lifetime ($\overline{\tau_m^b}$) recovered significantly in the bleached area, which demonstrates that the lifetime ($\overline{\tau_m^c}$) reduction is due to FRET and not caused by any other quenching process or photoconversion of the fluorophore (Biskup et al., 2004; Tramier et al., 2006; Hoffmann et al., 2008). The fact that the $\overline{\tau_m^c}$ did not completely recover to donor-alone values is possibly due to partly bleached and/or photoconverted CrFP donor molecules, which can occur during the imaging and APB procedure (Hoffmann et al., 2008).

Extending the basic bimolecular FRET setup by tagging molecules with three spectrally overlapping fluorophores has been employed by others to study ternary molecule interactions. This approach, for example, was used to study the interactions and the composition of complexes composed of small molecules in vitro (Lee et al., 2007), to follow molecular interactions over distances greater than 10 nm (Haustein et al., 2003), and to visualize interactions between three genetically encoded fluorophore-tagged fusion proteins in vivo (Galperin et al., 2004). The fluorescence intensity-based FRET approaches used in these studies rely on alternating excitation of the fluorophores and subsequent measurements of fluorescence intensities in separate channels to distinguish direct FRET from two-step FRET between the partners under study. Extensive calculations, taking the various FRET contributions and corrections for spectral bleed-through into account, then provide information about intermolecular distances and complex composition. Another method combines bioluminescence resonance energy transfer with BiFC to follow the formation of protein complexes. Due to the low luminescence and fluorescence signals, this method cannot be used to study phenomena at (sub)cellular resolution (Gandia et al., 2008). Recently, BiFC has been used in combination with FRET to visualize the ternary Fos-Jun-nuclear factor of activated T cells (NFAT) complex in mammalian COS-1 cells. This study, which paralleled our own experiments, demonstrated the formation of the heterooligomeric NFAT complex and the establishment of a ternary protein complex between Fos-Jun heterodimers and the NF-κB subunit p65 (Shyu et al., 2008a, 2008b). Here, we further corroborated the validity of this approach by employing FLIM, which is a more precise method to determine FRET and, unlike intensity-based approaches such as sensitized emission and APB, independent of fluorophore concentrations (Biskup et al., 2007).

Practical Implications for Conducting BiFC-FRET Measurements in Plant Cells

BiFC-FRET determination by APB or FLIM has caveats that should be considered when setting up a three-protein-interaction study. The drawbacks of using the BiFC system to monitor protein-protein interactions were discussed above and elsewhere (Hu et al., 2002; Held et al., 2008; Kerppola, 2008) and include, among others, the irreversibility of complex formation, which may stabilize specific as well as unspecific protein-protein interactions. Another implication of the irreversibility of BiFC complex formation is that, with respect to two of the partners, ternary protein complexes can only be studied statically by BiFC-FRET analysis. Owing to the high energy that is required to dissociate a BiFC complex (Kerppola, 2009), dynamic assemblies or disassemblies of the two BiFC partners cannot be resolved. In addition, high local concentrations of proteins in organelles or in the PM might promote the formation of BiFC complexes and therefore possibly visualize false-positive protein-protein interactions. A major drawback of FRET studies in general is that high numbers of photons are needed to reliably determine energy transfer. Therefore, relatively high concentrations of fluorophores, often only reached in an overexpression system, are required. These nonnatural concentrations might lead to ectopic protein localization or to altered cellular responses that may promote interactions between proteins and FRET due to molecular crowding.

For these reasons, FRET-based methods should include the proper (e.g. noninteracting) controls and should ideally be backed up by independent methods that demonstrate a protein-protein interaction (e.g. coimmunoprecipitation, far western blot, etc.). Ideally, BiFC-FRET measurements would be conducted using native expression levels (all three genes driven under control of their endogenous promoters) in a respective triple mutant background. For practical reasons, this "gold standard" will be impossible or impractical to obtain in most instances. Instead, nonnative transient gene expression, either mediated by *Agrobacterium tumefaciens* infiltration or protoplast transformation or following particle bombardment (as in this study), will remain common practice for fluorophore-based interaction studies (Bhat et al., 2006).

In addition, all FRET-based methods are prone to photophysical artifacts, like bleaching or photoconversion of the donor or acceptor molecule by prolonged exposure to light, which might not only change the intensity but may also reduce the lifetime of fluorophores with a multiexponential fluorescence decay such as CrFP and cyan fluorescent protein (Kremers et al., 2006; Tramier et al., 2006; Hoffmann et al., 2008; Villoing et al., 2008). This requires again proper controls or an independent method to confirm the interaction. One possibility is to combine FLIM with APB, as demonstrated in this study (Fig. 5; Supplemental Fig. S5E). A major advantage of demonstrating FRET between a CrFP and reconstituted YFP by FLIM compared with intensity-based approaches (Galperin et al., 2004; Shyu et al., 2008a, 2008b) is that the method is independent of fluorophore concentrations and provides a more precise quantification of the interaction. On the other hand, it requires sophisticated equipment, which is not always available. As successfully shown here and by others, APB or sensitized emission measurements can be used to demonstrate BiFC-FRET (Shyu et al., 2008a, 2008b), which makes the method accessible to a wider range of the plant community.

Overexpression of Complementary SNARE Proteins Results in the Formation VLC Clusters

Complementary to our FRET studies, the presence of a ternary SNARE complex containing HvROR2 was demonstrated by biochemical means (Fig. 1). This shows by an independent method that HvROR2, like AtPEN1 in Arabidopsis (Kwon et al., 2008), forms ternary SNARE complexes in planta. With the tools available, it was impossible to demonstrate the presence of HvSNAP34 or HvVAMP721 in this complex. The visualized complexes may thus represent a mixture of the ternary SNARE complex composed of HvSNAP34, HvVAMP721, and HvROR2 and other HvROR2-containing SNARE complexes.

Coexpression of two or three SNARE partners fused to complementary halves of a split YFP molecule revealed the formation of VLC clusters that contain the respective interacting SNARE partners (Fig. 2, D–J). The VLCs are not present in cells expressing only one of the SNARE partners and therefore are the consequence of the co-overexpression of two or more distinct SNAREs. They colocalize with a CrFP-CAAX membrane marker, and a range of PM-resident proteins are targeted to the same location. It thus seems that PM proteins together with membrane material in transit through the secretory pathway get targeted to the VLCs by the action of the co-overexpressed SNAREs.

Notably, VLC formation was not influenced by the BiFC system (Supplemental Fig. S4, J–M). Thus, the formation of a complemented YFP moiety does not significantly inhibit vesicle fusion events, suggesting that the BiFC complexes retain the ability for the formation of functional ternary SNARE complexes. When coexpressed and challenged with *Bgh*, the fluorescent SNARE fusion proteins focally accumulated below the fungal appressorium and the primary germ tube (Fig. 3). Occasionally, the accumulation sites were not shaped as a sphere but as scattered spots surrounding the fungal appressorium (Fig. 3, E–H). This resembles the pattern observed for the accumulation of hydrogen peroxide upon fungal challenge, where patches of hydrogen peroxide-containing papillae surround the central wall apposition (An et al., 2006). In both cases, the patterns of accumulation are likely the result of transport processes toward fungal attack sites.

At present, it is unclear what the origin of the VLCs is. One possibility is that the overexpression of multiple SNAREs results in runaway vesicle fusion due to disequilibrium between vesicle fusion and dissociation by exceeding the capacity of the SNARE complex-resolving machinery. This might artificially increase the fraction of interacting SNARE partners in our experimental system. It is conceivable that proteins that are normally cotransported with the SNAREs (e.g. on or inside vesicles) would coaccumulate at the same locations during this process. Alternatively, the overexpression of complementary exocytotic SNAREs may trigger a chain of cellular events that otherwise only occurs upon a biotic stress stimulus. With respect to their molecular composition, the VLC clusters could thus represent either an intracellular congregation of PM-resident proteins and vesicular compartments into an extremely large multiprotein complex (PM microdomain; Bhat et al., 2005) or the exaggerated formation of multivesicular bodies (Meyer et al., 2009).

CONCLUSION

Taken together, our findings demonstrate the technical feasibility of combined BiFC-FRET-FLIM and BiFC-FRET-APB measurements to monitor the existence of ternary protein complexes in living plant cells. We envisage future variations of this basic setup by the employment of multicolor fluorescence complementation analysis (Hu and Kerppola 2003; Jach et al., 2006;

Lee et al., 2008; Waadt et al., 2008) combined with FRET to visualize higher order complex formation. By choosing proper combinations of interacting proteins and respective split fluorophores and applying a triple FRET method as described by Galperin et al. (2004) or spectral/multichannel FLIM complexes, up to five interacting proteins can possibly be visualized.

MATERIALS AND METHODS

DNA Constructs

The expression vectors used in this study were constructed using Gateway technology (Invitrogen; www.invitrogen.com), unless stated otherwise. The pUCSPYNE, pUCSPYCE, pESPYNE, and pESPYCE vectors harboring N- and C-terminal halves of enhanced YFP (Walter et al., 2004; Schütze et al., 2009) were adapted to be Gateway compatible.

Microscopy

Fluorescence microscopy was carried out with a Zeiss LSM510 META confocal microscope (www.zeiss.com). A 40× Plan-Apochromat (Zeiss) water-immersive lens with a numerical aperture of 1.2 was used. CrFP or YFP was excited with the 458- or 514-nm laser line of an argon-ion laser, respectively. Fluorescence and excitation light were separated by a dual dichroic mirror, which reflected both the 458- and 514-nm laser lines. A second dichroic NFT515 filter was used to split the emission light into the CrFP and YFP detection channels. The CrFP fluorescence was selected by a 480- to 520-nm bandpass filter, and YFP fluorescence was recorded in META detector channels corresponding to the wavelength range from 526 to 569 nm. mCherry and FM 4-64 were excited by the 543-nm laser line of the helium-neon laser. Excitation and emission light were separated by a 543-nm dichroic filter. mCherry fluorescence was selected by a 565- to 615-nm bandpass filter, and FM 4-64 fluorescence was filtered by a 650- to 710-nm bandpass filter. To better separate the fluorescence of the coexpressed fluorophores, the measurements were performed in independent tracks exciting only one fluorophore at a time.

BiFC-FRET-APB

The same beam paths as mentioned above were used. The bleaching was performed as a time series with three image scans before bleaching and three or more images after bleaching. YFP was bleached by iteratively scanning a selected area of the cell 80 times with the 514-nm laser line of the argon-ion laser at a laser power of 178 μW in the focal plane and a pixel dwell time of 2.6 μs. The images were analyzed with Image J 1.42 (National Institutes of Health). Background signal was subtracted, and the FRET efficiency was calculated according to

$$E = 1 - \frac{I_{DA}}{I_D} \quad (1)$$

where I_{DA} is the intensity of the donor in the presence of the acceptor (i.e. before bleaching of the acceptor) and I_D is the intensity of the donor in the absence of the acceptor (i.e. after bleaching of the acceptor; for details, see Supplemental Materials and Methods S1). An average FRET efficiency was calculated from the three images taken immediately after the bleach.

Fluorescence Lifetime Microscopy

Fluorescence lifetime imaging microscopy was essentially performed as described previously (Bhat et al., 2005; Shen et al., 2007). In brief, a mode-locked titanium-sapphire laser (Chameleon; Coherent) was tuned to a wavelength of 840 nm for two-photon excitation of CrFP and tuned to 910 nm for YFP excitation. A dichroic 650KP beam splitter was used to separate excitation and emission light. Emission light was directed to the NDD port of the confocal laser scanning microscope. A BG39 filter (Schott) was used to block reflected excitation light, and a 465- to 495-nm or a 540- to 580-nm bandpass filter was used to select CrFP or YFP fluorescence, respectively. Single-photon events were detected with a multichannel plate photomultiplier (R3809U-52; Hamamatsu Photonics), which was connected to a SPC730 module (Becker and Hickl; www.becker-hickl.com) for time-correlated single-photon counting. For image acquisition, the area of interest was scanned continuously. The time-correlated single-photon-counting module was synchronized to the scan via the FrameSync, LineSync, and PixelSync signals of the confocal laser scanning microscope. The temporal resolution of this setup was better than 50 ps (full width half maximum).

An acquisition time of 120 s was sufficient to accumulate histograms of the fluorescence decay with a resolution of 128 × 128 pixels and 256 time channels. The histograms were analyzed with SPC-Image 2.9.1 software (Becker and Hickl) and our own software routines written in MATLab (MathWorks; for more details, see Supplemental Materials and Methods S1). Both software versions used the "iterative reconvolution method" to fit a monoexponential or biexponential decay function to the data. The parameters were approximated by a modified Levenberg-Marquardt algorithm, and the goodness of a fit was judged by the value of the reduced χ^2_v. To limit the number of parameters in a biexponential decay function to be fit, the second lifetime component was fixed to the average donor lifetime found in the donor-only measurements performed during the same session. A fit was regarded to be acceptable when $\chi^2_v < 1.2$. To visualize the lifetime distribution over the cell, average lifetimes were color coded.

In the case of a biexponential fit, amplitude-weighted mean lifetimes (τ_m) were calculated according to $\tau_m = A_f\tau_f + A_s\tau_s$, where A_f and A_s are the relative amplitudes of the fast and slow lifetime components, respectively. Mean lifetimes (τ^c_m) for an individual cell were calculated by averaging over the amplitude-weighted mean lifetimes ($\tau_{m,i}$) of all pixels (i), taking into account their intensity (I_i): $\tau^c_m = \sum_i I_i\tau_{m,i} / \sum_i I_i$. Mean lifetimes ($\overline{\tau^c_m} = \sum_j^n \tau^c_{m,j}/n$) for a series of measurements (j) are presented as means ± SD based on more than 10 cells from three or more independent experiments. In contrast to a monoexponential decay model, the use of a biexponential decay model consistently yielded $\chi^2_v < 1.2$ for the combinations showing FRET and therefore is regarded as the proper model to describe the lifetime decay data.

By comparing the lifetime of the donor in the presence of the acceptor τ^c_{DA} with the lifetime measured in the absence of the acceptor $\overline{\tau^c_D}$, the FRET efficiency can be calculated:

$$E = 1 - \frac{\tau^c_{DA}}{\overline{\tau^c_D}} \quad (2)$$

As fluorescence lifetimes are independent of the concentration of the fluorophores, FRET and control measurements can be carried out in different cells (for more details, see Supplemental Materials and Methods S1).

Supplemental Data

The following materials are available in the online version of this article.

Supplemental Figure S1. Additional details of subcellular SNARE localization.

Supplemental Figure S2. Results of screening experiments for fluorescent complexes of SNARE proteins fused to complementing halves of a split YFP.

Supplemental Figure S3. Coexpression of the three complementary barley SNARE partners with HvMLO, HvLTP, HvPIP2, or HvCytb561 leads to association of these proteins to VLCs.

Supplemental Figure S4. Coexpression of the complementary Arabidopsis SNAREs AtPEN1, AtSNAP33, and AtVAMP722 also results in association of the SNARE proteins to VLCs.

Supplemental Figure S5. Exemplary fluorescence emission spectra and fluorescence decay curves.

Supplemental Figure S6. Exchanging the donor molecule in the ternary SNARE complex abolishes FRET.

Supplemental Figure S7. In planta visualization of ternary SNARE complex formation by combined BiFC-FRET-FLIM in Arabidopsis leaf epidermal cells.

Supplemental Table S1. Fluorescence lifetimes and energy transfer efficiencies using a monoexponential fit.

Supplemental Materials and Methods S1.

ACKNOWLEDGMENTS

We thank Sacco de Vries and Adrie Westphal for help with the CrFP-CAAX cloning as well as Marc Hallstein and Anja Reinstädler for technical assistance. We thank Klaus Harter for providing the vectors for the BIFC system. Helpful suggestions for the improvement of the manuscript by the anonymous reviewers are acknowledged.

Received November 17, 2009; accepted January 8, 2010; published January 13, 2010.

LITERATURE CITED

An QL, Ehlers K, Kogel KH, van Bel AJE, Hückelhoven R (2006) Multivesicular compartments proliferate in susceptible and resistant MLA12-barley leaves in response to infection by the biotrophic powdery mildew fungus. New Phytol **172:** 563–576

Assaad FF, Qiu JL, Youngs H, Ehrhardt D, Zimmerli L, Kalde M, Wanner G, Peck SC, Edwards H, Ramonell K, et al (2004) The PEN1 syntaxin defines a novel cellular compartment upon fungal attack and is required for the timely assembly of papillae. Mol Biol Cell **15:** 5118–5129

Bhat RA, Lahaye T, Panstruga R (2006) The visible touch: *in planta* visualization of protein-protein interactions using fluorophore-based methods. Plant Methods **2:** 12

Bhat RA, Miklis M, Schmelzer E, Schulze-Lefert P, Panstruga R (2005) Recruitment and interaction dynamics of plant penetration resistance components in a plasma membrane microdomain. Proc Natl Acad Sci USA **102:** 3135–3140

Biskup C, Zimmer T, Benndorf K (2004) FRET between cardiac Na^+ channel subunits measured with a confocal microscope and a streak camera. Nat Biotechnol **22:** 220–224

Biskup C, Zimmer T, Kelbauskas L, Hoffmann B, Klocker N, Becker W, Bergmann A, Benndorf K (2007) Multi-dimensional fluorescence lifetime and FRET measurements. Microsc Res Tech **70:** 442–451

Bracha-Drori K, Shichrur K, Katz A, Oliva M, Angelovici R, Yalovsky S, Ohad N (2004) Detection of protein-protein interactions in plants using bimolecular fluorescence complementation. Plant J **40:** 419–427

Chen Y, Mills JD, Periasamy A (2003) Protein localization in living cells and tissues using FRET and FLIM. Differentiation **71:** 528–541

Clegg RM (1996) Fluorescence resonance energy transfer. *In* XF Wang, B Herman, eds, Fluorescence Imaging Spectroscopy and Microscopy. Chemical Analysis Series, Vol 137. John Wiley & Sons, New York, pp 179–251

Collins NC, Thordal-Christensen H, Lipka V, Bau S, Kombrink E, Qiu JL, Hückelhoven R, Stein M, Freialdenhoven A, Somerville SC, et al (2003) SNARE-protein-mediated disease resistance at the plant cell wall. Nature **425:** 973–977

Dale RE, Eisinger J, Blumberg WE (1979) The orientational freedom of molecular probes: the orientation factor in intramolecular energy transfer. Biophys J **26:** 161–193

Galperin E, Verkhusha VV, Sorkin A (2004) Three-chromophore FRET microscopy to analyze multiprotein interactions in living cells. Nat Methods **1:** 209–217

Gandia J, Galino J, Amaral OB, Soriano A, Lluis C, Franco R, Ciruela F (2008) Detection of higher-order G protein-coupled receptor oligomers by a combined BRET-BiFC technique. FEBS Lett **582:** 2979–2984

Haustein E, Jahnz M, Schwille P (2003) Triple FRET: a tool for studying long-range molecular interactions. ChemPhysChem **4:** 745–748

Heese M, Gansel X, Sticher L, Wick P, Grebe M, Granier F, Jurgens G (2001) Functional characterization of the KNOLLE-interacting t-SNARE *At*SNAP33 and its role in plant cytokinesis. J Cell Biol **155:** 239–249

Held MA, Boulaflous A, Brandizzi F (2008) Advances in fluorescent protein-based imaging for the analysis of plant endomembranes. Plant Physiol **147:** 1469–1481

Hink MA, Bisseling T, Visser AJ (2002) Imaging protein-protein interactions in living cells. Plant Mol Biol **50:** 871–883

Hoffmann B, Zimmer T, Klocker N, Kelbauskas L, Konig K, Benndorf K, Biskup C (2008) Prolonged irradiation of enhanced cyan fluorescent protein or Cerulean can invalidate Forster resonance energy transfer measurements. J Biomed Opt **13:** 031205

Hu CD, Chinenov Y, Kerppola TK (2002) Visualization of interactions among bZIP and Rel family proteins in living cells using bimolecular fluorescence complementation. Mol Cell **9:** 789–798

Hu CD, Kerppola TK (2003) Simultaneous visualization of multiple protein interactions in living cells using multicolor fluorescence complementation analysis. Nat Biotechnol **21:** 539–545

Jach G, Pesch M, Richter K, Frings S, Uhrig JF (2006) An improved mRFP1 adds red to bimolecular fluorescence complementation. Nat Methods **3:** 597–600

Jahn R, Scheller RH (2006) SNAREs: engines for membrane fusion. Nat Rev Immunol **7:** 631–643

Kerppola TK (2008) Bimolecular fluorescence complementation (BiFC) analysis as a probe of protein interactions in living cells. Annu Rev Biophys **37:** 465–487

Kerppola TK (2009) Visualization of molecular interactions using bimolecular fluorescence complementation analysis: characteristics of protein fragment complementation. Chem Soc Rev **38:** 2876–2886

Kremers GJ, Goedhart J, van Munster EB, Gadella TW Jr (2006) Cyan and yellow super fluorescent proteins with improved brightness, protein folding, and FRET Forster radius. Biochemistry **45:** 6570–6580

Kwon C, Neu C, Pajonk S, Yun HS, Lipka U, Humphry M, Bau S, Straus M, Kwaaitaal M, Rampelt H, et al (2008) Co-option of a default secretory pathway for plant immune responses. Nature **451:** 835–840

Leabu M (2006) Membrane fusion in cells: molecular machinery and mechanisms. J Cell Mol Med **10:** 423–427

Lee LY, Fang MJ, Kuang LY, Gelvin SB (2008) Vectors for multi-color bimolecular fluorescence complementation to investigate protein-protein interactions in living plant cells. Plant Methods **4:** 24

Lee NK, Kapanidis AN, Koh HR, Korlann Y, Ho SO, Kim Y, Gassman N, Kim SK, Weiss S (2007) Three-color alternating-laser excitation of single molecules: monitoring multiple interactions and distances. Biophys J **92:** 303–312

Lipka V, Kwon C, Panstruga R (2007) SNARE-Ware: the role of SNARE-domain proteins in plant biology. Annu Rev Cell Dev Biol **23:** 147–174

Meyer D, Pajonk S, Micali C, O'Connell R, Schulze-Lefert P (2009) Extracellular transport and integration of plant secretory proteins into pathogen-induced cell wall compartments. Plant J **57:** 986–999

Orthaus S, Biskup C, Hoffmann B, Hoischen C, Ohndorf S, Benndorf K, Diekmann S (2008) Assembly of the inner kinetochore proteins CENP-A and CENP-B in living human cells. ChemBioChem **4:** 77–92

Osterrieder A, Carvalho CM, Latijnhouwers M, Johansen JN, Stubbs C, Botchway S, Hawes C (2009) Fluorescence lifetime imaging of interactions between Golgi tethering factors and small GTPases in plants. Traffic **10:** 1034–1046

Pajonk S, Kwon C, Clemens N, Panstruga R, Schulze-Lefert P (2008) Activity determinants and functional specialization of *Arabidopsis* PEN1 syntaxin in innate immunity. J Biol Chem **283:** 26974–26984

Periasamy A, Day RN (2005) Molecular Imaging: FRET Microscopy and Spectroscopy. Methods in Physiology Series. Oxford University Press, Oxford

Rizzo MA, Springer GH, Granada B, Piston DW (2004) An improved cyan fluorescent protein variant useful for FRET. Nat Biotechnol **22:** 445–449

Russinova E, Borst JW, Kwaaitaal M, Cano-Delgado A, Yin YH, Chory J, de Vries SC (2004) Heterodimerization and endocytosis of *Arabidopsis* brassinosteroid receptors BRI1 and *At*SERK3 (BAK1). Plant Cell **16:** 3216–3229

Schütze K, Harter K, Chaban C (2009) Bimolecular fluorescence complementation (BiFC) to study protein-protein interactions in living plant cells. Methods Mol Biol **479:** 189–202

Shah K, Gadella TW Jr, van Erp H, Hecht V, de Vries SC (2001) Subcellular localization and oligomerization of the *Arabidopsis thaliana* somatic embryogenesis receptor kinase 1 protein. J Mol Biol **309:** 641–655

Shah K, Russinova E, Gadella TW Jr, Willemse J, De Vries SC (2002) The *Arabidopsis* kinase-associated protein phosphatase controls internalization of the somatic embryogenesis receptor kinase 1. Genes Dev **16:** 1707–1720

Shaner NC, Steinbach PA, Tsien RY (2005) A guide to choosing fluorescent proteins. Nat Methods **2:** 905–909

Shen QH, Saijo Y, Mauch S, Biskup C, Bieri S, Keller B, Seki H, Ulker B, Somssich IE, Schulze-Lefert P (2007) Nuclear activity of MLA immune receptors links isolate-specific and basal disease-resistance responses. Science **315:** 1098–1103

Shu X, Shaner NC, Yarbrough CA, Tsien RY, Remington SJ (2006) Novel

chromophores and buried charges control color in mFruits. Biochemistry **45:** 9639–9647

Shyu YJ, Suarez CD, Hu CD (2008a) Visualization of AP-1 NF-kappaB ternary complexes in living cells by using a BiFC-based FRET. Proc Natl Acad Sci USA **105:** 151–156

Shyu YJ, Suarez CD, Hu CD (2008b) Visualization of ternary complexes in living cells by using a BiFC-based FRET assay. Nat Protoc **3:** 1693–1702

Thompson GA, Okuyama H (2000) Lipid-linked proteins of plants. Prog Lipid Res **39:** 19–39

Tonaco IA, Borst JW, de Vries SC, Angenent GC, Immink RG (2006) *In vivo* imaging of MADS-box transcription factor interactions. J Exp Bot **57:** 33–42

Tramier M, Zahid M, Mevel JC, Masse MJ, Coppey-Moisan M (2006) Sensitivity of CFP/YFP and GFP/mCherry pairs to donor photobleaching on FRET determination by fluorescence lifetime imaging microscopy in living cells. Microsc Res Tech **69:** 933–939

Villoing A, Ridhoir M, Cinquin B, Erard M, Alvarez L, Vallverdu G, Pernot P, Grailhe R, Merola F, Pasquier H (2008) Complex fluorescence of the cyan fluorescent protein: comparisons with the H148D variant and consequences for quantitative cell imaging. Biochemistry **47:** 12483–12492

Waadt R, Schmidt LK, Lohse M, Hashimoto K, Bock R, Kudla J (2008) Multicolor bimolecular fluorescence complementation reveals simultaneous formation of alternative CBL/CIPK complexes *in planta*. Plant J **56:** 505–516

Walter M, Chaban C, Schutze K, Batistic O, Weckermann K, Nake C, Blazevic D, Grefen C, Schumacher K, Oecking C, et al (2004) Visualization of protein interactions in living plant cells using bimolecular fluorescence complementation. Plant J **40:** 428–438

Weinthal D, Tzfira T (2009) Imaging protein-protein interactions in plant cells by bimolecular fluorescence complementation assay. Trends Plant Sci **14:** 59–63

Weninger K, Bowen ME, Chu S, Brunger AT (2003) Single-molecule studies of SNARE complex assembly reveal parallel and antiparallel configurations. Proc Natl Acad Sci USA **100:** 14800–14805

Zacharias DA, Violin JD, Newton AC, Tsien RY (2002) Partitioning of lipid-modified monomeric GFPs into membrane microdomains of live cells. Science **296:** 913–916

Zhang Z, Feechan A, Pedersen C, Newman MA, Qiu JL, Olesen KL, Thordal-Christensen H (2007) A SNARE-protein has opposing functions in penetration resistance and defence signalling pathways. Plant J **49:** 302–312